Electronic Supplementary Material (ESI) for Journal of Materials Chemistry A.

## Supporting Information

# Hierarchically structured, oxygen deficient, tungsten oxide morphologies for enhanced photoelectrochemical charge transfer and stability

*Peng Chen*[1], *Matthew Baldwin*[2], and *Prabhakar R. Bandaru*[1, 2, *]

[1]Program in Materials Science, [2]Center for Energy Research,

Department of Mechanical Engineering, University of California, San Diego, La Jolla, CA

*E-mail: pbandaru@ucsd.edu

## A. Surface morphology

Scanning electron microscopy (SEM) images, indicating the morphology of the other tested samples, *i.e., S1* and *S3*, in addition to that of sample *S2* – depicted in Fig. 1(b)

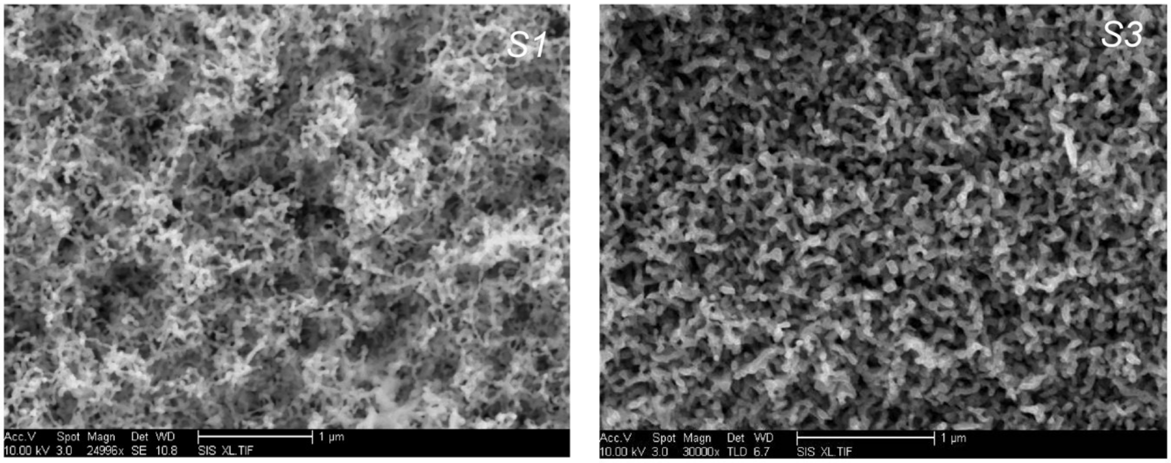

**Figure A1** SEM images of samples *S1* and *S3*.

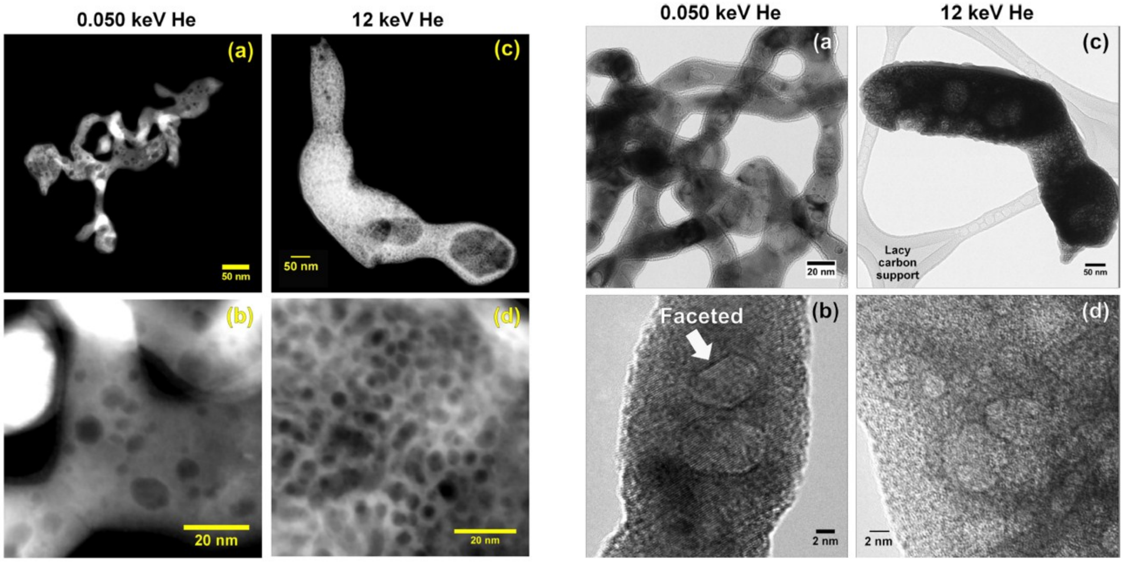

**Figure A2 (a)** Scanning transmission electron microscopy (STEM) - high angle annular dark field (HAADF), and **(b)** high-resolution transmission electron microscopy (HRTEM) based images of the fuzzy tungsten: (*from* K. Wang, …, M. J. Baldwin, *et al,* "*Morphologies of tungsten nanotendrils grown under helium exposure*", *Scientific Reports* 2017, *7*, 42315)

## B. X-ray diffraction (XRD)

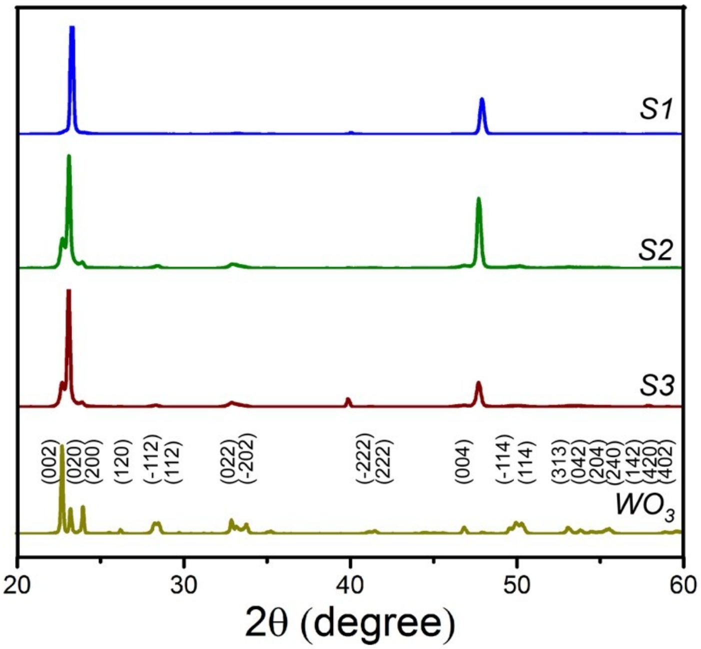

**Figure B1** XRD patterns for the samples reported in the paper. The specific peak assignments were taken from JCPDS (Joint Committee on Powder Diffraction Standards) files as well as through reference with published literature.

The XRD features of the ***reference*** sample (stoichiometric WO$_3$, without nanostructure) have been indexed with reference to monoclinic WO$_3$ phase (JCPDS standard card ID: 00-043-1035). The ***S1*** sample may also be indexed in correspondence to the monoclinic WO$_{2.83}$ phase (JCPDS standard card ID: 00-036-0103), with the (010) peak at 23.48°, the (020) peak at 48.08°, *etc.* For samples ***S2*** and ***S3***, the (010) peak at 23.27° with a shoulder (-1 0 16) at 24.16°, along with the broad peak ~30° for (-4 0 12) and a sharper peak at 40.80° for (-4 1 12) were in correspondence to the monoclinic WO$_{2.92}$ phase (JCPDS standard card ID: 00-030-1387)[1]. The peak at ~ 48° for *S2* seems to mainly originate from the WO$_{2.9}$ phase, accounting for the higher intensity, and implying more of such phase in this sample. The peak at ~ 40$^0$ seems to correspond to metallic W. Moreover, the presence of the (002) and (200) peaks related to WO$_3$ phases also seem to be present in these samples, indicating the occurrence of a mixture of phases[1–4].

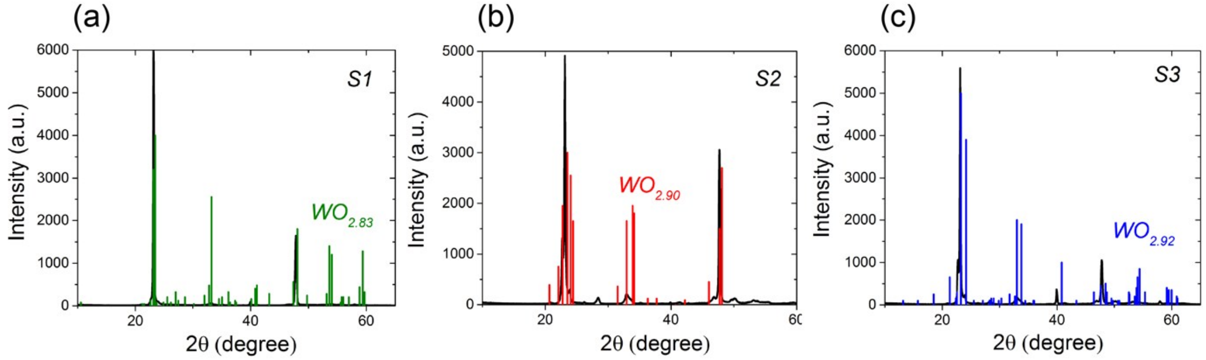

**Figure B2** XRD patterns for the samples reported in the paper. The specific peak assignments were taken from JCPDS (Joint Committee on Powder Diffraction Standards) files as well as through reference with published literature.

## C. X-ray photoelectron spectroscopy (XPS)

W 4*f* core level spectra are shown in **Fig. 2** (*main text*) and **Fig. C1**. $W^{6+}$ with peak positions related to W $4f_{7/2}$ at 35.90 eV and W $4f_{5/2}$ 38.05 eV can be recognized. We applied for the W $4f_{7/2}$ and W $4f_{5/2}$ peaks, (i) an area ratio of 4:3 (*i.e.,* per the multiplicity of the corresponding levels, which is $2j + 1$), (ii) assumed line widths to be equal, and (iii) peak positions corresponding to the binding energy difference ($\Delta BE$), where W $4f_{5/2}$ - W $4f_{7/2}$ = 2.1 eV[3]. A pronounced shoulder on the lower binding energy side of the $W^{6+}$ 4*f* signal was attributed to $W^{5+}$ $4f_{7/2}$ orbital at ~ (33 – 34) eV. Additionally, the position of $W^{4+}$ $4f_{7/2}$ peak is about 32 eV. W metal, indicated by W $4f_{7/2}$ peak is ~31.15eV. The XPS fitting results correspond well with the values reported in literature[2–4].

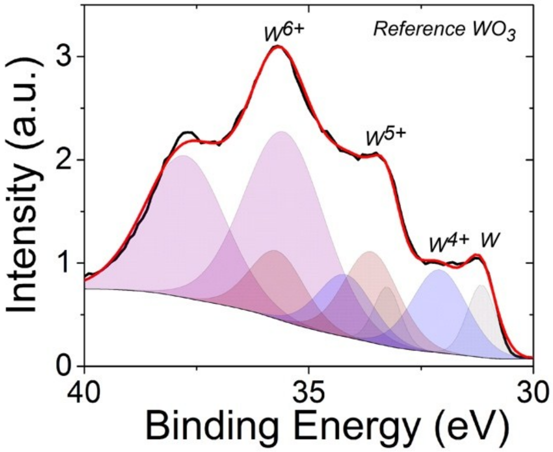

**Figure C1** XPS spectra of the *reference* $WO_3$ sample. Such a sample *does not* have the fuzzy structure, as indicated in Figure 1(b) of the main text.

**Evaluation of the ratio:**

$$N = \frac{WO_3}{WO_{3-x}} \sim \frac{W^{6+}}{W^{4+} + W^{5+}}$$

The areas of the peaks corresponding to the different oxidation states of W, i.e., $W^{4+}$, $W^{5+}$, and $W^{6+}$ were estimated from XPS spectra (as indicated in **Figure 2**) and used for computing the *N*.

**Table C1**: Samples considered through the ratio of $WO_3/WO_{3-x}$

| Sample | W oxidation state | $W4f_{7/2}$ BE (V) | FWHM (eV) | Relative amount (%) | $WO_3/WO_{3-x}$ (= $N$) |
|---|---|---|---|---|---|
| *S1* | 6+ | 35.95 | 1.707 | 45.61 | $1.01 \approx 1$ |
| | 5+ | 33.96 | 2.168 | 32.70 | |
| | 4+ | 31.88 | 1.256 | 12.61 | |
| | metal | 31.15 | 0.662 | 9.08 | |
| *S2* | 6+ | 35.94 | 1.907 | 63.63 | $2.13 \approx 2$ |
| | 5+ | 33.49 | 1.111 | 13.74 | |
| | 4+ | 32.04 | 1.293 | 16.19 | |
| | metal | 31.19 | 0.668 | 6.44 | |
| *S3* | 6+ | 35.76 | 1.582 | 71.43 | $3.10 \approx 3$ |
| | 5+ | 33.76 | 1.366 | 12.83 | |
| | 4+ | 32.07 | 1.356 | 10.20 | |
| | metal | 31.13 | 0.707 | 5.54 | |

We also note the following: *S1* – $WO_{2.6815}$ has 10.62% oxygen vacancies; *S2* – $WO_{2.7535}$ has 8.22% oxygen vacancies and *S3* – $WO_{2.8241}$ has 5.86% oxygen vacancies.

## D. Photoelectrochemical current measurements

Considering the linear scan voltammogram (LSV) of **Figure 3(a)**, the oxidation current on illumination was the largest for sample *S2*, with oxygen vacancies intermediate to samples *S1* and *S3*. Corresponding electrochemical measurements on the reference $WO_3$ sample (without nanostructural features) indicated a current density of ~ 0.5 mA/cm$^2$ compared with 1.7 mA/cm$^2$ of *S2*: **Figure D1 (a)**. Significantly smaller hysteretic behavior was observed for the reference sample. In contrast to *S2*, the stability of the reference sample steadily decreased through repeated cycling: **Figure D1 (b)**.

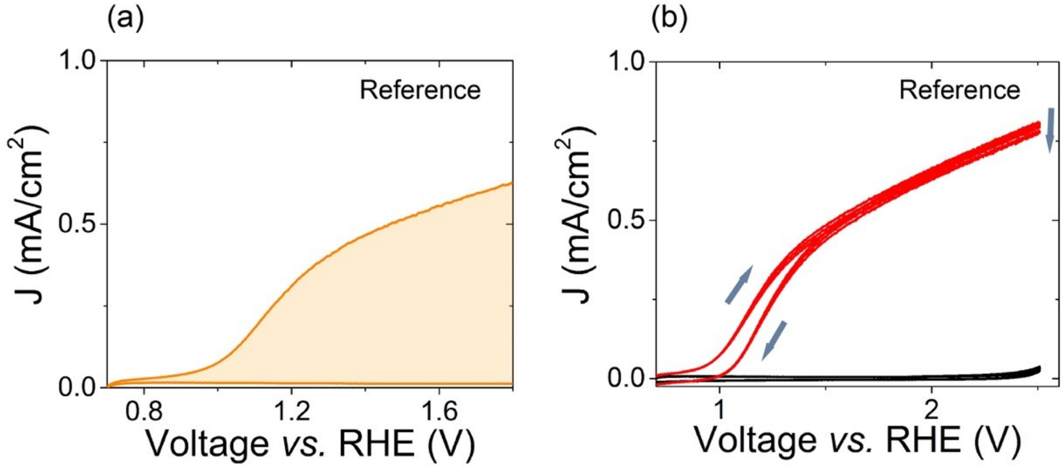

**Figure D1.** Photoelectrochemical measurement on reference sample **(a)** LSV – ***upper*** curve taken under sample illumination, ***lower*** curve for the *dark*/un-illuminated case; **(b)** CV measurement over three cycles indicates decreasing stability (***upper*** curve taken under sample illumination, ***lower*** curve for the *dark*/un-illuminated case).

Comparing the cyclic voltammograms of all the three samples, *i.e., S1 – S3*, it is seen that the area in the *J-V* or the *C-V* curve is largest for sample *S2*.

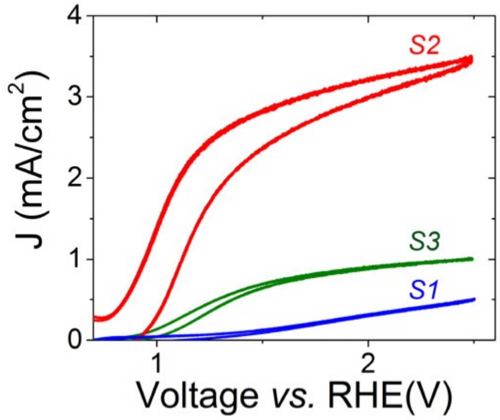

**Figure D2** Comparison of the cyclic voltammetry (CV) based characterization of samples *S1, S2,* and *S3* over ten cycles.

## E. Electrochemical impedance spectroscopy (EIS)

The EIS spectra for samples *S1* and *S3* are indicated below.

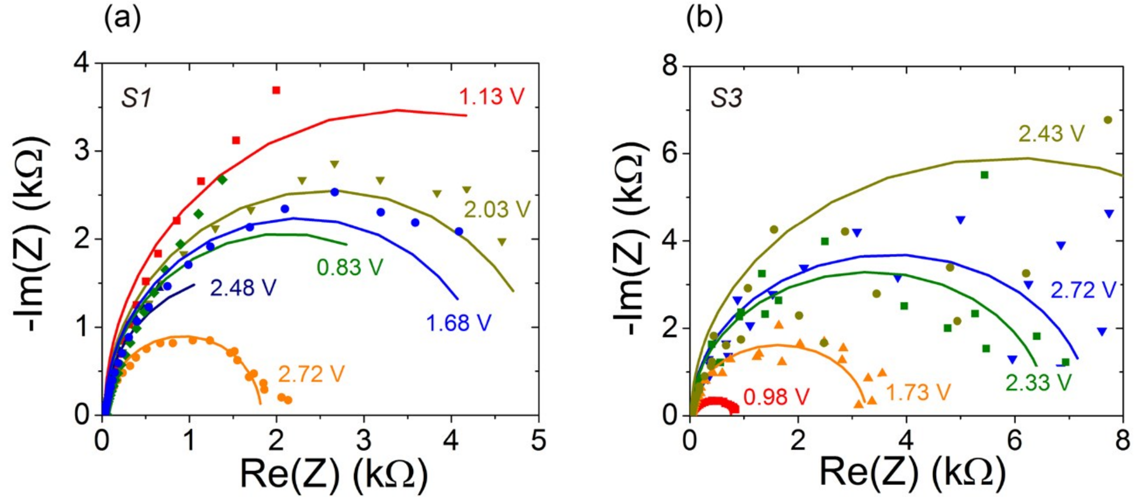

**Figure E1** Nyquist plot indicating the negative of the imaginary: -Im (Z) and Re(Z) components of the impedance for samples **(a)** *S1*, and **(b)** *S3* at various applied voltages (with respect to RHE).

Based on a Randles circuit based fitting model depicted in **Figure 4(b)**, kinetic information can be collected from EIS. Samples under illumination and in the dark exhibit different tendency in $R_{ct}$ vs. $V$ plots (as indicated through **Figure 4** in the text).

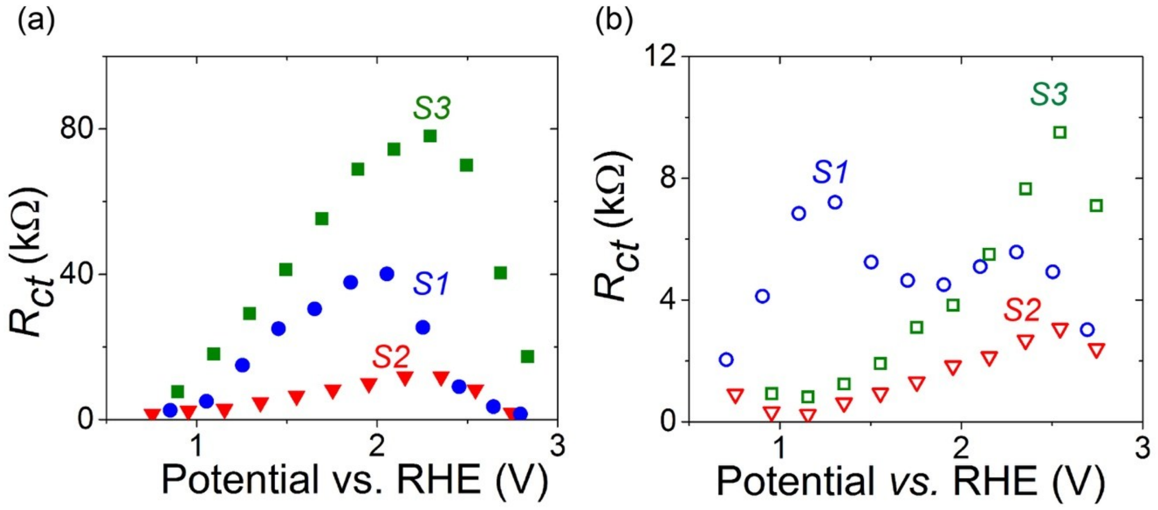

**Fig. E2** (a) $R_{ct}$ vs. $V$ (**dark**) (b) $R_{ct}$ vs. $V$ (**under illumination)** in $K_2SO_4$

**Table E1:** The peak $R_{ct}$ for the samples

| Sample | Dark-$R_{ct}$ (kΩ) | Light- $R_{ct}$ (kΩ) | Dark-Peak-$V_{app}$ (V) | Light-Peak-$V_{app}$ (V) |
|---|---|---|---|---|
| *S1* | 40 | 6 | 2.1 | 1.2 & 2.3 |
| *S2* | 10 | 3 | 2.3 | 2.7 |
| *S3* | 83 | 12 | 2.3 | 2.7 |

From **Figure E1** and **Table E1**, it may be inferred that the *S2* sample has the lowest $R_{ct}$, and is reduced when the sample was illuminated (*i.e.,* from ~ 10 kΩ to ~ 3 kΩ). Such reduction of the $R_{ct}$ under illumination was seen for all the samples. The voltage at which the peak $R_{ct}$ occurs is correlated to the energy at which the exchange current, say, for highly efficient photoelectrochemical oxidation of water, is a minimum. The shift of the $R_{ct}$ peak, when the sample is illuminated was also seen for all the samples and is related to the developed photovoltage. We also found an additional peak rising on *S1*. The potential of this peak is around half of the peaks we discussed previously. The reason for this peak is not clear, but it is possible to be a mid-gap defect level, as a new recombination center associated with oxygen vacancies[5]. Generally, oxygen vacancies are associated with electrons implying that samples with more (/less) number of vacancies have more (/less) number of electrons. Consequently, samples with more (/less) number of vacancies have smaller (/larger) associated $h^+$ (positive holes) charge carriers. We have determined that sample *S1* has the largest number of vacancies and hence the smallest number of $h^+$. A small $h^+$ concentration implies a reduced OER ($2H_2O + 4h^+ \rightleftharpoons O_2 + 4H^+$) capability, *i.e.,* due to inadequate number of carriers, and leads to a *diminished* OER related exchange current ($i_o$) and an increased $R_{ct}$ (which varies as $1/i_o$). Alternately, sample *S3* has the smallest number of vacancies and hence the largest number of $h^+$. A large $h^+$ concentration implies a relatively small area over which the $h^+$ could aggregate, from Equation (b) in Section 2.4, of the main text. Again, the OER exchange current is reduced and leads to an increased $R_{ct}$.

**References**

[1] G. Wang, Y. Ling, H. Wang, X. Yang, C. Wang, J. Z. Zhang, Y. Li, *Energy Environ. Sci.* **2012**, *5*, 6180.

[2] T. Singh, R. Muller, J. Singh, S. Mathur, *Appl. Surf. Sci.* **2015**, *347*, 448.

[3] S. Darmawi, S. Burkhardt, T. Leichtweiss, D. A. Weber, S. Wenzel, J. Janek, M. T. Elm, P. J. Klar, *Phys Chem Chem Phys* **2015**, *17*, 15903.

[4] J. Qian, Z. Peng, Z. Shen, Z. Zhao, G. Zhang, X. Fu, *Sci. Rep.* **2016**, *6*, 25574.